Atmos. Chem. Phys. Discuss., 12, 18605–18650, 2012
www.atmos-chem-phys-discuss.net/12/18605/2012/
doi:10.5194/acpd-12-18605-2012

Atmospheric Chemistry and Physics Discussions

New particle growth and shrinkage observed in subtropical environments

L.-H. Young[1], S.-H. Lee[2], V. Kanawade[2], T.-C. Hsiao[3], Y. L. Lee[4], B.-F. Hwang[1], Y.-J. Liou[1], H.-T. Hsu[5], and P.-J. Tsai[1]

[1]Department of Occupational Safety and Health, China Medical University, 91 Hsueh-Shih Road, Taichung 40402, Taiwan
[2]College of Public Health, Kent State University, 750 Hilltop Drive, Kent, OH 44240, USA
[3]Graduate Institute of Environmental Engineering, National Central University, 300 Jhongda Road, Jhongli City, Taoyuan County 32001, Taiwan
[4]Graduate Institute of Epidemiology and Preventive Medicine, National Taiwan University, 17 Xu-Zhou Road, Taipei 10020, Taiwan
[5]Department of Health Risk Management, China Medical University, 91 Hsueh-Shih Road, Taichung 40402, Taiwan

Received: 8 July 2012 – Accepted: 16 July 2012 – Published: 30 July 2012

Correspondence to: L.-H. Young (lhy@mail.cmu.edu.tw)

Published by Copernicus Publications on behalf of the European Geosciences Union.

Abstract

We present the first systematic analysis for new particle formation (NPF), growth and shrinkage of new particles observed at four different sites in subtropical Central Taiwan. A total of 14 NPF events were identified during 137 days of ambient measurements during a cold and warm season. The derived nucleation rates of 1 nm particles (J_1) and growth rates were in the range of 39.6–252.9 $cm^{-3} s^{-1}$ and 6.5–14.5 $nm h^{-1}$, respectively. The NPF events occurred on days either with low condensation sink (CS), increased morning traffic emissions and the breakup of nocturnal inversion layer (type A), or with high CS, minimum levels of primary traffic emissions and enhanced atmospheric dilution (type B). On non-event days, the particle number concentrations were mostly driven by traffic emissions. We have also observed shrinkage of new particles (type A-S and B-S), reversal of growth, during five out of the 14 NPF events. In intense shrinkage cases, the grown particles shrank back to the smallest measurable size of $\sim$ 10 nm, thereby creating a unique "arch-like" shape in the size distribution contour plot. The particle shrinkage rates ranged from 5.1 to 7.6 $nm h^{-1}$. The ratios of shrinkage-to-growth rates were mostly in the range of 0.40–0.65, suggesting that a large fraction of the condensable species that contributed to growth were likely semi-volatile. The particle shrinkage was related to air masses with low CS due to atmospheric dilution, high ambient temperature and low relative humidity and such atmospheric conditions may have facilitated the evaporation of semi-volatile species from the particles to the gas phase. Our observations show that the new particle growth may be a reversible process and the evaporating semi-volatile species are important for the growth of new particles to cloud condensation nuclei sizes.

1 Introduction

Atmospheric aerosols impact various aspects of human health, air quality and climate. Aerosol particles are also linked to short- and long-term cardiovascular disease and

ACPD
12, 18605–18650, 2012

mortality (Atkinson et al., 2010; Pope et al., 2009). Fine particles of diameters smaller than 2.5 µm ($PM_{2.5}$) can be more pertinent to health effects (Peng et al., 2009; Zanobetti and Schwartz, 2009). And, ultrafine particles (UFPs) in the size range of smaller than 100 nm can be even more toxic, as they exhibit unique physicochemical properties and deposit more efficiently in the alveolar region than larger particles (Nel, 2006). In ambient air, aerosol number concentrations are dominated by these UFPs.

Atmospheric UFPs are from two source processes, primary emissions and secondary formation. UFP particles are directly emitted from motor vehicles, particularly heavy-duty diesel engines (Morawska et al., 2008). For example, emission studies of heavy-duty diesel engines have shown that non-volatile UFPs in the exhaust are on the order of 10^7–10^8 cm^{-3} (Heikkilä et al., 2009; Young et al., 2012a), several orders of magnitude higher than ambient UFP concentrations. The secondary formation process that governs particle number concentrations is new particle formation (NPF). NPF involves nucleation (gas-to-particle conversion) and initial growth to sizes larger than ~ 3 nm detectable by current instruments (Kulmala, 2003). Once clusters formed via nucleation and become larger than the critical size, growth becomes spontaneous. Subsequent growth of freshly nucleated particles often persists for many hours under favorable atmospheric conditions (e.g. under low pre-existing aerosol particle and high concentrations of low volatility compounds) to become larger than 50 nm to act as cloud condensation nuclei. Unlike motor vehicle emissions that are limited to urban areas, NPF events have been observed in all types of environments, including rural, coastal, urban areas and boreal forest (Kulmala et al., 2004). More recently, Hallar et al. (2011) showed frequent NPF, correlated with UV irradiance, in background free tropospheric air. Studies have shown that the number concentrations of freshly nucleated particles at the start of NPF typically are in the range of 10^3–10^4 cm^{-3}, but under certain conditions, for example in SO_2-enriched plumes and coastal areas, they can be higher than 10^4 cm^{-3} (Kulmala et al., 2004; Holmes, 2007; Bzdek and Johnston, 2010). Its spatial scale in regional events can extend beyond tens and up to several hundred kilometers (Stanier et al., 2004; Salma et al., 2011). The large scale of NPF

ACPD
12, 18605–18650, 2012

have been recognized as a potentially significant contributor to the global CCN production (Merikanto et al., 2009). Most of NPF observations have so far been made at mid- and high-latitude regions of Northern Hemisphere (Kulmala et al., 2004) and the measurements in subtropical and tropical regions are sparse.

The favorable conditions and mechanisms leading to NPF and growth have been proposed for various atmospheric conditions. Kulmala et al. (2004), Bzdek and Johnston (2010), Hegg and Baker (2009), Holmes (2007), and Kulmala and Kerminen (2008) have illustrated the dynamic relationships among the nucleating (condensable) vapors, pre-existing aerosol densities, particle growth rates and nucleation rates. These studies also showed that NPF occurs when there are excess condensable vapors for the freshly nucleated particles to grow large without being scavenged by pre-existing aerosols. Zhang et al. (2012) reviewed recent advances in nucleation and growth and provided insights of these processes at the molecular level. Due to its low volatility at typical atmospheric temperatures, gas-phase sulfuric acid (H_2SO_4) is the most important nucleating vapor (Kuang et al., 2008; Kerminen et al., 2010; Sipila et al., 2010). Ternary species such as ammonia (NH_3), amines and other organic compounds can also enhance the nucleation rate by stabilizing critical clusters (Benson et al., 2011; Erupe et al., 2011; Yu et al., 2012; Zhang et al., 2004).

Growth of new particles are governed by coagulation, condensation of low volatility and semi-volatile vapors, and heterogeneous reactions. Coagulation of freshly nucleated particles decreases the particle number and increases the modal size. However, its effect on particle growth is less importance unless the number concentration and nucleation rate exceeds $\sim 10^5\,cm^{-3}$ and $10^4\,cm^{-3}\,s^{-1}$, respectively (Anttila et al., 2010; Lehtinen et al., 2007). And, such conditions are rather uncommon but have been observed in polluted urban air or industrial plumes or coastal areas. Yue et al. (2010) showed that intra- and extra-modal coagulation contributed 34 ± 17 % to particle growth during events with formation rates of 2–13 $cm^{-3}\,s^{-1}$ in Beijing. Because condensation growth is strongly suppressed owing to the Kelvin effect for small particles, only vapors of low vapor pressure contribute to growth of freshly nucleated particles. Condensation

ACPD
12, 18605–18650, 2012

of H_2SO_4 and subsequent stabilization by H_2O is considered irreversible under typical atmospheric conditions (Zhang et al., 2009). However, field studies have found that H_2SO_4 condensation alone often fails to fully account for the observed particle growth (Stolzenburg et al., 2005; Yue et al., 2010), and it is possible that other semi-volatile organic vapors contribute to growth of new particles (Laaksonen et al., 2008; Zhang et al., 2009; Riipinen et al., 2011; Pierce et al., 2012). The Kelvin-effect barrier can be overcome by heterogeneous reactions, which can facilitate a subsequent condensation of organic vapors (Zhang and Wexler, 2002). Also, amines and particulate-phase H_2SO_4 or organic acids lead to the formation of low volatility aminium salts that contribute to particle growth (Smith et al., 2010).

Particle shrinkage can also occur due to evaporation of condensed species if condensation or chemical reactions involved in particle growth are reversible. Suggested reversible processes with regard to new particle growth include the formation of aldol products and glyoxal oligomers in H_2SO_4 particles, and the physical adsorption of alcohols by H_2SO_4 solution (Zhang et al., 2012). In addition, particle-phase oxidation may result in enhanced volatilization of organic aerosols (Kroll et al., 2006; Molina, 2004). Modeling studies showed that vehicle-emitted particles smaller than 40 nm can shrink when the gas-phase concentration decreases (Zhang and Wexler, 2004; Jacobson et al., 2005). In Hong Kong urban air, Yao et al. (2010) observed particle shrinkage following several NPF events and suggested that the particle shrinkage was related to the evaporation of organic components and ammonium nitrate. Recently, Backman et al. (2011) reported similar observations in São Paulo, Brazil, and suggested that the decrease of vapor concentrations by changes in atmospheric conditions could occur more rapidly than the decrease of vapor pressure by photochemical oxidation. Therefore, the net effect is the evaporation of the condensed phase to the gas phase.

Here, we have characterized the NPF events observed in various subtropical environments (urban, coastal, mountain and downwind). A notable result is intense particle shrinkage of new particles. Young et al. (2012b) have previously characterized the

ACPD
12, 18605–18650, 2012

spatiotemporal variability of particles in the size range from 10–1000 nm at the same sites, and this study focuses on the NPF growth and shrinkage.

2 Experimental

2.1 Observation sites

The observation sites, instruments, meteorological conditions and data reduction methods are described in detail in Young et al. (2012b). Observations were made at four air quality monitoring sites in the Central Taiwan, a subtropical island country situated on the western edge of the Pacific Ocean and off the southeastern coast of mainland China. The study sites are located 20–50 km apart in the Central Taiwan Air Quality Management District (CTAQMD) of ~ 7400 km^2 and nominally represent urban, coastal, mountain and downwind area (Fig. 1).

The urban site is in the center of the Taichung City basin, which has approximately 2 610 000 registered vehicles, ranking the 3rd in the country (Taiwan Ministry of Transportation and Communications, http://www.motc.gov.tw/). Among these vehicles, 65 % are 4-stroke and 2-stroke scooters (ratio = 7 : 3), 30 % are mostly gasoline-powered passenger cars, and the remaining 5 % are trucks, buses and other types of vehicles. The coastal site is situated 4.8 km to the western coastline of Taiwan and 9 km south to the largest coal-fired power plant in Taiwan. The mountain site is located in a relatively rural basin; its east is the Central Mountain Ranges of height 2–3 km. The downwind site is near the southern border of the CTAQMD, 44 km to the southeast of the Taichung urban area. The prevailing northeasterly winds during winter months were conducive for transport of air pollutants from the upwind urban area to the downwind site.

The sampling campaigns were conducted consecutively at these four sites from October 2008 to January 2009 (cold season) and from August 2010 to October 2010 (warm season). The major meteorological differences between the cold and warm season include the average ambient temperature (20.6 vs. 27.6 °C), prevailing wind

ACPD
12, 18605–18650, 2012

direction (NNW vs. W) and accumulated precipitation (57.4 vs. 283.6 mm). The air quality was considered poorer during the cold season than the warm season, especially the all-sites hourly-average particulate matter smaller than 10 µm (PM_{10}, 57.1 µg m^{-3} during the warm season vs. 37.0 µg m^{-3} during the cold season) ($PM_{2.5}$, 37.2 vs. 24.2 µg m^{-3}), NO_x (23.9 vs. 15.4 ppb) and SO_2 (3.8 vs. 2.9 ppb). During the entire study period, we collected a total 26 075 aerosol number-size distributions over 137 effective sampling days (with the data coverage of ~ 92.5 %).

2.2 Sampling and instrumentation

The aerosol measurement systems at all four observation sites were nearly identical and housed inside air-conditioned trailers. Ambient air was drawn through the site rooftop with a flow rate of 8 l min^{-1} (lpm) via a 3-m vertical glass tube (ID = 2 cm, outer diameter OD = 2.54 cm). The outdoor section of the glass tube (2.5 m long) was shielded inside an aluminum tube. A short stainless steel forward-facing sampling probe was inserted into the indoor section of the remaining glass tube (0.5 m). A small portion of the sample air (0.3 lpm) was then taken into the scanning mobility particle sizer (SMPS) through the sampling probe with a 1.5-m conductive tubing. The diffusion loss to the glass and conductive tubing was estimated to be ~ 15 % for the smallest measureable particles of 11.1 nm, based on Baron and Willeke (2001). However, no loss corrections were made to the measured data. The air conditioners inside the trailers were activated only when the indoor temperature exceeded 31 °C. As a result, the sample air temperature basically followed the ambient air temperature. There were no water condensation issues with the sampling tube.

The particle number size distributions were measured with SMPS (GRIMM Aerosol Technik, Gmbh, Germany, Model 5.500) (e.g. Heim et al., 2004). The SMPS consists of an Am-241 neutralizer (Model 5.522), a long Vienna-type differential mobility analyzer (L-DMA; Model 55-900) and a butanol-based condensation particle counter (CPC; Model 5.403). With the default set up, the inner electrode of the L-DMA is positively

ACPD
12, 18605–18650, 2012

charged. The CPC has a 50 % counting efficiency for particles as small as 4.5 nm, with the saturator and condenser temperature set at 40 °C and 15 °C, respectively. The SMPS was set to down-scan 6 min and 26 s from 10 000 V to 5 V plus a wait-time of 34 s, thus producing one average particle number size distribution every 7 min. The detectable aerosol mobility diameters range from 11.1 to 1083.3 nm (44 size bins) with a sheath and sample flow of 3 lpm and 0.3 lpm, respectively. For simplicity, we hereafter refer to the measureable size range as 10–1000 nm (as opposed to 11.1 to 1083.3 nm).

On-site air quality and meteorological data were obtained from the monitoring sites and validated by the Taiwan Environmental Protection Administration (TW EPA, 2009). At the sites, PM_{10} and $PM_{2.5}$ were continuously monitored by means of β-ray attenuation, SO_2 by UV fluorescence, NO_x by chemiluminescence, CO by nondispersive IR, and O_3 by UV absorption. Meteorological parameters used in the present study include temperature, relative humidity (RH), wind speed, wind direction and UV index (UVI). The UVI (1 UVI = 100 $J\,m^{-2}$) is used here as an indicator of solar intensity. The evolution of the mixing height was estimated using the web-based real-time environmental applications and Display system (READY) from the Air Resources Laboratory of NOAA (http://ready.arl.noaa.gov/READYamet.php). The archive data were from the Global Data Assimilation System of National Centers for Environmental Prediction, which has a temporal and spatial resolution of 3 h and 1° of latitude and longitude, respectively.

2.3 NPF event classification

Aerosol size distribution data were subjected to quality control and assurance procedures that screen for abnormal size distributions, whereas the gas pollutants and meteorological data were obtained directly from the monitoring sites maintained and validated by the TW EPA. Only less than 0.1 % of aerosol data were identified as outliers and not included in the analysis. Following, the size segregated particle number concentrations were derived by integrating the number concentrations of particles between 10–25, 25–100, 10–100 and 100–1000 nm. These concentrations hereafter are

ACPD
12, 18605–18650, 2012

denoted as N_{10-25}, N_{25-100}, N_{10-100} and $N_{100-1000}$, respectively. Hourly aerosol data were then computed to synchronize with the gas pollutants and meteorological data.

Identification of NPF events was made visually on a daily basis according to a set of distinct features in the temporal evolution of the aerosol number size distributions (e.g. Dal Maso et al., 2005; Stanier et al., 2004). An NPF event is characterized by a substantial increase of N_{10-25} followed by intense particle growth over a course over 1.5 h, in which the nucleation and growth rates can be determined with a good confidence level. The NPF events were further classified into two classes based on the start time of apparent NPF (t_{start}). The end time of NPF (t_{end}) is defined as the time when the particle growth stopped. Type A and B events are those with t_{start} before and after ~ 09:00 LT, respectively. The t_{start} is an important parameter as it indirectly relates to the specific atmospheric conditions (such as mixing height, temperature, and RH) and the traffic emission source strength, both of which exhibit strong temporal dependence. If the NPF was followed by intense particle shrinkage, it is then denoted as type A-S or type B-S.

2.4 Determination of nucleation, growth rate and condensation sink

The empirical nucleation rates (J) during the NPF events were determined by an inverse modeling, as well as a simplified approximation. The two methods base on the general dynamic equation (GDE) in describing the evolution of aerosol size distribution (Seinfeld and Pandis, 2006). The inversion model known as Particle Growth and Nucleation (PARGAN) is described in detail elsewhere (Verheggen and Mozurkewich, 2006; Erupe et al., 2010; Metzger et al., 2010). The online version of PARGAN is available at http://www.personal.kent.edu/~slee19/softwares.htm. In brief, the model implements a non-linear regression analysis of the GDE to fit the temporal evolution of the measured particle number size distributions. As such, the growth rate (GR_{PARGAN}) as a function of time can be determined and then used to estimate the time when the nucleation begins. Such highly time-resolved approach is therefore sensitive to any noise or variability in the measured size distributions. In this work, we assume the critical

ACPD
12, 18605–18650, 2012

cluster has a diameter of 1 nm (Sipila et al., 2010). The J_1 is then derived by integrating particle losses from the time of nucleation to the time of measurement. This approach thus differs from others, because the GR_{PARGAN} is determined using a range of size intervals instead of total or modal particle number concentration and the J_1 is calculated solely on the basis of the measured size distributions, hence independent of any nucleation theories or parameterizations.

We also calculated the formation rate of 10 nm particles using a simplified GDE method (Dal Maso et al., 2005):

$$J_d = \frac{dN_{10-25}}{dt} + F_{coag} + F_{growth} \quad (1)$$

where N_{10-25} is the number concentration of nucleated particles, F_{coag} is the loss of particles due to coagulation, and F_{growth} is the flux of particles out of the nucleated particle size range. The smallest measurable particle size is ~ 10 nm in this study, while the upper size range of the nucleated particle is set at 25 nm. Hence, the formation rate of 10 nm particles is hereafter denoted as J_{10}. Assuming the homogeneous air mass with a constant source rate, dN_{10-25}/dt was determined by a linear fit between N_{10-25} and t. In the same fashion, the modal growth rate (GR_{MOD}) was determined between particle mode diameter (D_{mode}) and t. F_{coag} was computed from (Dal Maso et al., 2005):

$$F_{coag} = N_{NUC} \sum_j K_{ij} N_j \quad (2)$$

where the summation of $K_{ij} N_j$ is also known as the coagulation sink. N_j is the number concentration of size bin j. K_{ij} is the coagulation coefficient between size bin i (i.e. the reference) and j, and takes the below form (Seinfeld and Pandis, 2006):

$$K_{ij} = 2\pi(d_i + d_j)(D_i + D_j)\beta_F \quad (3)$$

where d is the midpoint diameter of a size bin, D and β_F are the size-dependent diffusion coefficient and Fuchs correction factor, respectively. It is noted that particle

ACPD
12, 18605–18650, 2012

loss due to self-coagulation is neglected because of its minor contribution to NPF and growth, compared with inter-coagulation and condensation, especially in polluted environments (Anttila et al., 2010). F_{growth} is also neglected for simplicity, but in the present study the particles appear to grow relatively fast (e.g. to the upper size boundary within the first several hours). As a result, this method likely underestimated the actual J_{10}.

Condensation sink (CS) is a measure of loss rate of H_2SO_4 vapor on pre-existing particles and is proportional to the surface area density of aerosol particles. Elevated pre-existing particles can suppress aerosol nucleation by scavenging freshly nucleated particles and condensable vapors. Assuming H_2SO_4 as the condensable species, the CS in the transition regime was calculated as follows (Erupe et al., 2010):

$$CS = 2\pi D_v \sum_j d_j \beta_{m,j} N_j \quad (4)$$

where D_v is the diffusion coefficient of H_2SO_4 ($0.104\,cm^2\,s^{-1}$) estimated by the FSG-LaBas method (Lyman et al., 1990), and β_m is the size dependent transitional correction factor (Fuchs and Sutugin, 1971).

3 Results and discussion

3.1 Characteristics of NPF events in central Taiwan

Among the 137 sampling days at the four study sites, we identified 14 intense NPF events. The NPF types, meteorological and air quality conditions during these events are summarized in Table 1. As shown, 11 of them took place in the warm season (August–September) and three in the cold season (December–January). In addition, nine events occurred at the urban site, four at the downwind site, one at the coastal site, and none at the mountain site. The mountain site had the highest average $PM_{2.5}$ of 47.7 and 36.9 $\mu g\,m^{-3}$, whereas the PM_{10} were 66.7 and 49.3 $\mu g\,m^{-3}$ in the cold and warm season, respectively (Young et al., 2012b). The high PM levels thus may have

ACPD
12, 18605–18650, 2012

suppressed the NPF. All events, except one (17 December 2008), started before ~ 10:30 LT and all ended before ~ 15:00 LT. These t_{start} and t_{end} are similar to those observed in Beijing, China (Wu et al., 2007), Pittsburg, PA, USA (Stanier et al., 2004) and Hyytiälä, Finland (Boy and Kulmala, 2002).

Nine events are type A events (growth started before 9 a.m. with the influence of traffic) and five are type B events (growth started after 9 a.m. without the influence of traffic). The duration (Δt) from the start of NPF to the end of particle growth took between 1.5 and 5 h. It is notable that eight out of the nine type A events took place over consecutive days (10–17 August 2010) at the urban site in the warm season (Appendix A, Fig. A1). Surprisingly, in five of the NPF events, the growth was immediately followed by intense particle shrinkage. Two shrinkage events were found during type A events in the warm season (type A-S), and three during type B events with two in the warm season and one in the cold (type B-S).

On the event days, the ambient temperature and RH were below 18.4 °C and 66.5 % in the cold season, whereas mostly above 27.0 °C and 69.3 % in the warm season. The wind speeds (WS) were considerable stagnant (mostly < 1.3 m s^{-1}) during all the event days except the one at the coastal site. The prevailing winds were from the northeast in the cold season whereas from the south or east in the warm season. The daily $PM_{2.5}$ were typically below 20 µg m^{-3}, substantially lower than the annual average value of the hourly $PM_{2.5}$ (35.8 µg m^{-3}). Only three event days had $PM_{2.5}$ above 26.4 µg m^{-3} and up to 46.6 µg m^{-3}. The daily CS and SO_2 were in the range of 1.6–3.9 × 10^{-2} s^{-1} and 2.0–4.6 ppb, respectively. On the event days, the above $PM_{2.5}$ and CS were similar to those observed in Pittsburg, PA (Stanier et al., 2004) and Beijing, China (Wu et al., 2007), whereas the SO_2 were lower than in these two cited locations.

3.2 Nucleation, growth and shrinkage rates

The PARGAN-derived nucleation rates (J_1) during NPF events at the urban site were in the range of 131.9–252.9 cm^{-3} s^{-1}, whereas at the coastal and downwind sites they

ACPD
12, 18605–18650, 2012

were lower and in the range of 39.6–113.1 $cm^{-3} s^{-1}$ (Table 2). The observed J_1 are inline with the modeled median nucleation rates of 311 $cm^{-3} s^{-1}$ and 18.1 $cm^{-3} s^{-1}$ in polluted boundary layer and the rural/continental background, respectively (Anttila et al., 2010; Kulmala et al., 2004), yet substantially lower than the nucleation rates of $3 \times 10^5 - 5 \times 10^7$ $cm^{-3} s^{-1}$ in coastal areas (Pirjola et al., 2002). Using the same PARGAN method (Erupe et al., 2010; Kanawade et al., 2012), the median J_1 of $\sim$ 11 $cm^{-3} s^{-1}$ in semi-rural Kent, USA, are substantially lower than the present study. This difference may be due to the substantially higher SO_2 and other possible nucleating vapors emitted from traffic at the present study sites. On the other hand, based on the growth rates and Fuchs surface area, Iida et al. (2008) estimated the J_1 in Mexico City and New Delhi were 1900–3000 $cm^{-3} s^{-1}$ and $\sim$ 1300 $cm^{-3} s^{-1}$, respectively. These values are substantially higher than the J_1 in this study. The latter two megacities are substantially more polluted with respect to SO_2 and PM than the present study area (Gurjar et al., 2008; Raga et al., 2001).

The approximation-derived formation rates of 10 nm particles (J_{10}) during NPF events at the urban site were 7.0–29.8 $cm^{-3} s^{-1}$, whereas at the coastal and downwind sites they were 4.4–14.5 $cm^{-3} s^{-1}$. The coagulation losses, F_{coag} in Eq. (1), of the newly-formed 10–25 nm particles at the urban site accounted for 45–80 % of the derived J_{10}, whereas at the coastal and downwind sites its contributions to J_{10} were more variable, between 28–85 %. Overall, these losses on average accounted for 60 ± 17 % of the J_{10}. This shows that the apparent particle flux (dN/dt) alone would have largely underestimated the J_{10}. The observed J_{10} in this study are generally higher than that reported in the studies summarized by (Kulmala et al., 2004) over a large number of measurements sites worldwide. Recent studies showed that formation rates of 3 nm particles (J_3) in Hong Kong Beijing, Shangdianzi and New Delhi were 1.8–5.1 $cm^{-3} s^{-1}$, 2–81.4 $cm^{-3} s^{-1}$, 0.7–72.7 $cm^{-3} s^{-1}$ and 3.3–13.9 $cm^{-3} s^{-1}$, respectively (Mönkkönen et al., 2005; Shen et al., 2011; Wu et al., 2007; Yao et al., 2010; Yue et al., 2010).

ACPD
12, 18605–18650, 2012

The PARGAN-derived growth rates (GR_{PARGAN}) and approximation-derived GR_{MOD} at the urban site were 6.5–9.5 nm h^{-1} and 6.7–23.9 nm h^{-1}, respectively. At the coastal and downwind sites, they were 6.7–14.5 nm h^{-1} and 7.4–15.4 nm h^{-1}, respectively. The GR_{PARGAN} on average accounted for 82 ± 30 % of the GR_{MOD}, similar to the percentage shown by Erupe et al. (2010). This consistency provides additional confidence with the PARGAN derived J_1, which were estimated from GR_{PARGAN}.

On five event days, the GR_{MOD} during particle shrinkage were between −5.1 and −7.6 nm h^{-1}, which were slightly smaller than that between −8.2 and −10.7 nm h^{-1} observed in Hong Kong (Yao et al., 2010). The ratio of shrinkage-to-growth rate for each shrinkage event day was in the range of 0.40–0.65, with an exception for the shrinkage event on the 7 September 2010 during which the ratio was 1.06. These ratios suggest that 40–65 % of the originally condensed chemical species were evaporated from the particles to gas phase under our atmospheric conditions. Such percentages are surprising similar to the percentages of new particle growth (54–59 %) due to NO_3^-, NH_4^+ and organics reported by Bzdek et al. (2012), with the remaining 41–46 % growth contributed by sulfate, which is considered non-volatile under typical atmospheric conditions. In an extreme case on the 7 September 2010 at the present downwind site, the near unity ratio indicates that the growth and shrinkage of new particles was completely reversible.

A closer examination of the size distribution data reveals that the two shrinkage events (3 January 2009 and 5 September 2010) showed simultaneous decrease of particle size and N_{10-25}, similar to the Hong Kong shrinkage events. However, the other three shrinkage events (12 August, 16 August and 7 September 2010) showed decreasing particle size with increasing N_{10-25}. Furthermore, unlike those reported in Hong Kong, the grown particles can shrink back to the smallest measurable size of ∼ 10 nm. As a result, the new particle growth and shrinkage creates a unique "arch-like" shape in the size distribution contour plot.

ACPD
12, 18605–18650, 2012

3.3 Diurnal variations of condensation sink, particle number and air pollutants

Figure 2 shows the diurnal variations of the average mixing height, NO_x CO, CS, SO_2 and N_{10-100} concentrations on non-event (n = 123), type A (n = 9) and type B (n = 5) event days. After the sunrise at ~ 06:00 LT, the mixing height grew gradually in the beginning and more rapidly after 08:00 LT (Fig. 2a). It then typically reached a maximum between 11:00–14:00 LT. After the sunset at ~ 18:00 LT, the mixing height decreased to 200–400 m. The peak concentrations of CO and NO_x in the morning and evening (Fig. 2b, c) were a result of increased traffic during rush-hour periods and decreased mixing height. Accordingly, the cutoff t_{start} of 09:00 LT clearly shows that the start of type A events between 07:00–09:00 LT was in the midst of traffic rush hours and nocturnal inversion breakup. Therefore, the start of type A events was likely linked to traffic emissions of nucleating/condensable vapors and new particles. On the other hand, the start of type B events occurred between 09:30–12:00, near the end of both traffic rush hours and inversion breakup. This is the time of day when the mixing layer is almost fully developed and characterized by minimum levels of primary traffic emissions due to enhanced atmospheric dilution and dispersion. Furthermore, the solar intensity is also strongest during midday hours. It is therefore suggested that the start of type B events was not related to primary traffic emissions, but due to elevated secondary photochemical species of low volatility during the midday.

The CS on type A event days were a factor of ~ 2 lower than that on non-event and type B event days, especially the periods preceding the NPF (i.e. before 09:00 LT) (Fig. 2d). This shows that type A events typically occurred on clean days whereas type B events occurred on relatively more polluted days. After 09:00 LT, the CS showed significant divergence in different types of days. On the type B event days, CS dropped rapidly to a minimum at 11:00 LT. It is noted that such decrease rate was steeper than that on non-event days. This underscores the importance of atmospheric dilution in the start of type B NPF events on more polluted days. Mönkkönen et al. (2005) showed that the start of all NPF events coincided with minimum levels of CS in highly polluted

ACPD
12, 18605–18650, 2012

Asian mega city. On the contrary, CS on the type A event days increased immediately after 09:00 LT and reached a maximum at ~ 12:00 LT. The increase of CS on both types of event days was a result of the particle growth following the start of NPF. However, such increase occurred after 09:00 LT for type A events and after 11:00 LT for type B events. Finally, it is noted that the diurnal variations of $N_{100-1000}$ were nearly identical to that of CS, suggesting dominant contributions of accumulation particles to the CS. As a result, the data on $N_{100-1000}$ were not presented here to avoid repetition.

The diurnal variations of SO_2 were similar between non-event and event days (Fig. 2), although the levels were generally higher on non-event days (Fig. 2e). Before 12:00 LT, the maximum SO_2 was at 09:00 LT on non-event and type B event days. Since the peak time coincided with CO and NO_x, the former SO_2 peaks were attributable to direct traffic emissions. On type A event days, there was also a traffic-related SO_2 peak at 08:00 LT. In addition, type A and B event days both had another SO_2 peak at 10:00 LT and 12:00 LT, respectively. These SO_2 peaks, however, were more intense and unlikely related to traffic emissions, based on the times of peak, yet they were positively correlated with elevated N_{10-100} on event days (Fig. 2f). This suggests a possible connection between the NPF and SO_2, which were likely emitted from sources other than motor vehicles, such as power plant and industrial plumes, and then transported to the study sites or mixed down from aloft (Stanier et al., 2004). After 12:00 LT, a consistent SO_2 maximum occurred at 15:00–16:00 LT for both non-event and event days. Although not related to the identified NPF and growth events, it occasionally did coincide with elevated levels of N_{10-25} (e.g. see the case studies on the 12 and 17 August 2010).

Below, the size-segregated particle number concentrations during NPF events are compared to average levels at the same sites and the same periods given by Young et al. (2012b). The average N_{10-25} during the NPF and growth events were in the range of 1.2–4.0 $\times$ 10^4 cm^{-3} (Table 2), which are ~ 1.7 to 5.7 times higher than average levels of 0.7 $\times$ 10^4 cm^{-3}. The average N_{25-100} were in the range of 1.3–3.3 $\times$ 10^4 cm^{-3}, which are ~ 1.2 to 3.0 times higher than average levels of 1.1 $\times$ 10^4 cm^{-3}. It is clear that the NPF events resulted in substantial increases of the N_{10-100} (i.e. UFPs). On

ACPD
12, 18605–18650, 2012

non-event days, the diurnal variations of N_{10-100} were nearly identical to those of NO_x and CO (Fig. 2f). This result indicates that the particle number variability on non-event days was largely driven by traffic emissions. Similar traffic-related N_{10-100} peaks (i.e. ones that occurred at ~ 08:00 LT) were also observed at a downwind site in urban Budapest, Hungary (Salma et al., 2011). On type A event days, the N_{10-100} after 07:00 LT increased sharply to a maximum at 10:00 LT and then decreased gradually throughout the day. It is notable that this N_{10-100} peak lagged for 1–2 hours after the morning traffic-related N_{10-100} peak. This result suggests that the elevated UFP at 10:00 LT was not emitted directly from motor vehicles but formed shortly afterwards in the atmosphere. On average, the N_{10-100} of 7.5×10^4 cm^{-3} during NPF was ~ 3.6 times higher than that of 2.1×10^4 cm^{-3} emitted from the morning traffic. Furthermore, the integral N_{10-100} over type A event days was 83 % and 47 % higher than that on non-event and type B event days, respectively. On type B event days, the temporal pattern and levels of N_{10-100} in the morning were similar to those on non-event days. After 10:00 LT, the N_{10-100} on type B event days deviated largely away from that on non-event days and increased considerably to a maximum of 3.8×10^4 cm^{-3} at 13:00 LT. This NPF-related N_{10-100} peak was also not related to traffic, and was ~ 1.8 times higher than the morning traffic-related N_{10-100}. The integral N_{10-100} over type B event days was 25 % higher than that on non-event days, indicating type B events had a smaller impact on UFPs than that by type A events.

The above results indicate that type A events were preferred on days that begin with low pre-existing particles (hence CS), which likely in turn allowed the start of NPF ~ 2 h earlier than that of type B events. Type B events on the other hand were preferred on days that involve intense midday atmospheric dilution, which appears to be a necessary factor because of the elevated pre-existing particles prior to events. Nevertheless, the start of both types of events coincided with minimum levels of CS. The possible involvement of SO_2, hence H_2SO_4 is implicated in the start of both type A and B events. However, the lower or comparable SO_2 on event days than on non-event days suggests that SO_2 was not a limiting factor for NPF. Salma et al. (2011) found that the SO_2 (yearly

ACPD
12, 18605–18650, 2012

median 2.6 ppb) is always in excess for NPF in Budapest, Hungary. In this study, there are several possible reasons to this rather counterintuitive preference for low SO_2: first, the minimum SO_2 of ~ 2.0 ppb at the study sites is already sufficient for NPF. Second, the rate-limiting step in the production of H_2SO_4 involves the oxidation of SO_2 by OH. Therefore, elevated SO_2 alone does not necessarily warrant increased production of H_2SO_4. Third, elevated SO_2 are often accompanied with elevated CS, particularly in urban air or industrial plumes. In this study, for example, the daily SO_2 were positively correlated with CS, $PM_{2.5}$, NO_x and CO with correlation coefficients of 0.38, 0.30, 0.26 and 0.23, respectively. The elevated CS as well as co-pollutants may have scavenged a significant fraction of H_2SO_4, hence suppressing the NPF and growth. It is also found that the SO_2 possibly involved in NPF events were not from local traffic emissions but from power plant or industrial plumes and then transported to the study sites or mixed down from aloft (Stanier et al., 2004). Finally, the NPF events resulted in substantial increases of the UFPs, especially during the daytime hours, and that such impact from type A events was stronger than type B events.

3.4 Case study of type A NPF: growth of new particles before 9 a.m. with traffic influence

Type A events were the most common (9 out of 14 NPF events observed) in the present air quality management district. All type A events (except one) were observed in the warm season at the urban site with high traffic emissions. On the 17 August 2010, the N_{10-25}, CS, CO and NO_x started to increase from 05:00 LT and then reached a maximum at ~ 08:00 LT due to the increased traffic emissions during rush hours (Fig. 3). Such traffic-related N_{10-25} at 08:00 LT had a maximum of 1.7×10^4 cm^{-3}. Between 08:00 and 09:00 LT, the size distribution contour plot shows a significant decrease of particles larger than 50 nm at 09:00 LT, indicating strong atmospheric dilution on this day. As a result, the primary pollutants CO, NO_x and CS began to decrease and reached a minimum at ~ 11:00 LT. At about the same time, the N_{10-25} sharply increased from 1.5×10^4 cm^{-3} to 5.8×10^4 cm^{-3} at 10:00 LT. The N_{10-25} peak coincided

ACPD
12, 18605–18650, 2012

with a SO_2 peak of 4.3 ppb, indicating the involvement of H_2SO_4 (as opposed to direct traffic emissions) in NPF. The high level of N_{10-25} was then followed by intense particle growth from 11 to 62 nm over a duration of ~ 4 h. The J_1 and GR_{PARGAN} during the first 2 h of the event varied around 200 $cm^{-3}\,s^{-1}$ and 5 $nm\,h^{-1}$, respectively. The GR_{PARGAN} then increased to ~ 15 $nm\,h^{-1}$ in the final few hours. Prior to 10:00 LT, the relatively light winds came from the southeast under a cloudless and sunny condition (9.7 UVI). The O_3 had a maximum of 65 ppb at 13:00 LT. Near the end of the type A event, the winds became westerly and another N_{10-25} peak was observed at 15:00 LT. Unlike the morning event, this afternoon particle formation event was plume-related because of the concurrently elevated primary pollutants SO_2 (17 ppb), NO_x (36 ppb) and CO (0.5 ppm), and a decrease of O_3 (37 ppb). In addition, there was no particle growth following the particle formation, possibly because of the extremely high CS (7.1×10^{-2} s^{-1}) and decreased photochemical activities (low UVI and O_3).

3.5 Case study of type B NPF: growth of new particles after 9 a.m. without traffic influence

Three type B events were observed in the cold season and two type B events were observed in the warm season. As described in Sect. 2.3, the start time of type B event is after 09:00 LT or even near the midday. This time of day is typically characterized by relatively low concentrations of primary pollutants CO and NO_x, but elevated O_3 and mixing height. For example, on the 3 December 2008, the N_{10-25}, CO and NO_x started to increase from 05:00 LT and then reached a maximum at ~ 08:00 LT (Fig. 4). The traffic-related N_{10-25} at 08:00 LT had a maximum of 1.4×10^4 cm^{-3}, which is similar to that observed on type A event days. After 08:00 LT, the CO and NO_x then decreased substantially due to decreased source strength and increased mixing height. Strong atmospheric dilution caused the CS to drop to a minimum of 2.2×10^{-2} s^{-1} at 13:00 LT. At about the same time, the N_{10-25} increased sharply from 0.5×10^4 cm^{-3} to 3.5×10^4 cm^{-3} within an hour. The only pollutant that coincided with the N_{10-25} peak was

ACPD
12, 18605–18650, 2012

the SO_2 (5 ppb). The NPF event was then followed by intense particle growth from 11 to 39 nm during the following two hours. The J_1 reached as high as $\sim 300\,cm^{-3}\,s^{-1}$ at 12:30 LT, whereas the GR_{PARGAN} were in the range of 2–10 $nm\,h^{-1}$. The southeasterly winds in the morning were stagnant ($< 0.6\,m\,s^{-1}$). Afterwards the wind direction changed to northerly and the wind speed increased significantly to above $1\,m\,s^{-1}$. The UVI indicates it was a cloudless sunny day. Despite the maximum UVI of 5.2 at 12:00 LT is relatively weak (compared to Fig. 3d), the O_3 peak of 84 ppb at 16:00 LT was significantly higher than that at the urban site in the warm season (e.g. Fig. 3c; 65 ppb O_3). This suggests that photochemical activities could be quite strong at the downwind site in the cold season. The termination of the midday NPF event at 16:00 LT coincided with elevated CS ($5.5 \times 10^{-2}\,s^{-1}$) and SO_2 (6.2 ppb). This result suggests that the polluted air may have suppressed the NPF by scavenging the precursor vapors and freshly nucleated particles. There were elevated N_{10-25} of $1.7 \times 10^4\,cm^{-3}$ during the morning and evening rush hours. Comparing the N_{10-25} levels between the traffic at about $\sim$ 08:00 LT and NPF after $\sim$ 09:00 LT, the intensity of UFP production via the secondary pathway was generally stronger than the primary pathway.

3.6 Case studies of particle shrinkage events

Particle shrinkage events were identified during five out of the 14 NPF events. Two shrinkage events were observed at the urban site, two at the downwind site and one at the coastal site. Detailed descriptions of each shrinkage event are presented below.

3.6.1 Urban site

On the 12 August 2010 at the urban site in the warm season, the start of type A NPF occurred at $\sim$ 08:00 LT in the midst of traffic rush hour (Fig. 5). It was then immediately followed by intense particle growth from 11 to 51 nm until 12:30 LT. The maximum N_{10-25} of $5.2 \times 10^4\,cm^{-3}$ at 10:00 LT was preceded by a local minimum CS of $1.7 \times 10^{-2}\,s^{-1}$, and it was correlated with a SO_2 peak of 3.6 ppb. The median J_1 and GR_{PARGAN} were

ACPD
12, 18605–18650, 2012

216.3 $cm^{-2} s^{-1}$ and 7.4 $nm h^{-1}$, respectively. Between 12:30 and 16:00 LT, the D_{mode} and CS decreased from 32 to 11 nm and 3.1 × 10^{-2} to 1.5 × 10^{-2} s^{-1}, respectively. It is notable that the shrinkage occurred during periods with the strongest atmospheric dilution (max. mixing height 590 m), highest ambient temperature (max. 34 °C) and lowest relative humidity (min. 61 %). The continuous decrease of CS as well as CO and NO_x during the shrinkage period suggests that the site was not impacted by local primary emissions. Meanwhile, the N_{10-25} and SO_2 were increasing with time. The N_{10-25} reached another maximum of 5.1 × 10^4 cm^{-3} near the end of the shrinkage. The GR_{MOD} during the growth and shrinkage were 10.7 and −5.6 $nm h^{-1}$, respectively. The winds of below 1.7 $m s^{-1}$ were mild throughout the day. The winds were from the south before 12:00 LT, but then changed to westerly during the shrinkage period. The change of wind direction was accompanied with a slight increase of wind speed and the appearance of cloud clover, as indicated by the sudden drop of UVI at 14:00 LT. The maximum O_3 was 51 ppb. The SO_2 peak of 3.4 ppb during the shrinkage period was of particular interest as the rise of SO_2 levels was simultaneously observed at three other air quality monitoring sites near the urban basin (Appendix A, Fig. A2).

On the 16 August 2010, the type A NPF between 08:30 and 13:00 LT was followed by intense particle shrinkage (Fig. 6). Between 13:00 and 15:00 LT, the D_{mode} and CS decreased from 30 to 11 nm and 3.4 × 10^{-2} to 2.0 × 10^{-2} s^{-1}, respectively. Again, the shrinkage occurred during periods with the strongest atmospheric dilution (max. mixing height 698 m), highest ambient temperature (max. 34 °C) and lowest relative humidity (min. 57 %). The diurnal variations of air pollutants (including N_{10-25}) and meteorological parameters on this day were very similar to the previously described shrinkage event on the 12 August 2010. For example, the CO and NO_x peaks at 08:00 LT and 19:00 LT, respectively, and the O_3 peak during midday hours. The wind speed and direction as well as their changes over the course of the day were nearly identical. Given such meteorological conditions, the data from a nearby monitoring site (12 km to the

ACPD
12, 18605–18650, 2012

northwest) shows a significant impact of SO_2 (21.2 ppb) on the study area at 15:00 LT, as did on the 12 August 2010.

These results suggest that the SO_2-enriched and low-CS air mass due to atmospheric advection and mixing may in turn have caused another NPF event, while the enhanced atmospheric dilution and hot/dry ambient conditions favor the evaporation of semi-volatile species from the particles to the gas phase. The former explains the increasing N_{10-25} whereas the latter results in the decreasing D_{mode}.

3.6.2 Coastal site

On the 3 January 2009 at the coastal site in the cold season, the type B NPF between 10:30 and 13:00 LT was followed by intense particle shrinkage (Fig. 7). During this period, the N_{10-25} increased rapidly from 1.0×10^4 cm^{-3} to 2.5×10^4 cm^{-3}. SO_2 also increased from 2.1 to 4.0 ppb. Afterwards, the particles grew from 11 to 36 nm. The median J_1 and GR_{PARGAN} were 98.8 cm^{-2} s^{-1} and 14.5 nm h^{-1}, respectively. Then the N_{10-25} gradually decreased to 0.6×10^4 cm^{-3} by 19:00 LT; the D_{mode} decreased from 30 to 11 nm between 14:00 and 17:00 LT. The GR_{MOD} during the growth and shrinkage were 7.8 and 5.1 nm h^{-1}, respectively. The elevated CS, CO and NO_x at 16:00 LT indicate an impact of polluted air. However, it did not affect the apparent particle shrinkage. Although not measured onsite, a nearby monitoring site (8.3 km to the southeast) shows that it was a cloudless sunny day with the maximum UVI of 4.1 between 12:00 and 13:00 LT. The prevailing north-northeasterly winds were strong (> 4 m s^{-1}), cold and stable throughout the event day. It is also notable that the temperature increased from a minimum 12 °C to a maximum 20 °C between 12:00 and 16:00 LT. These results suggest that the strong dilution due to elevated wind speed and large temperature rise were likely the driving forces leading to the evaporation of semi-volatile species from the particles to the gas phase. However, unlike those at the urban site, the above particle shrinkage is characterized by a simultaneous decrease of D_{mode} and N_{10-25}.

ACPD
12, 18605–18650, 2012

3.6.3 Downwind site

On the 5 and 7 September 2010 at the downwind site in the warm season, two type B NPF events between 10:00 and 13:00 LT were followed by particle shrinkage (Figs. 8 and 9). The trend of decreasing D_{mode} with increasing N_{10-25} was similar to that observed at the urban site, although the intensity was considerably weaker. On the 5 September 2010, the GR_{MOD} during the growth and shrinkage were 15.4 and $-7.1\,nm\,h^{-1}$, respectively. On the 7 September 2010, the GR_{MOD} were 7.4 and $-7.6\,nm\,h^{-1}$, respectively. In particular, the nearly equal growth and shrinkage rate in the latter case suggests that the initially condensed chemical species completely evaporated by the end of the shrinkage period. However, the particle shrinkage terminated at sizes of $\sim$ 20 nm, as opposed to $\sim$ 11 nm shown in the previous case studies. The shrinkage also occurred during periods with the strongest atmospheric dilution (elevated wind speed), highest ambient temperature (max. 32 °C) and lowest relative humidity (min. 58 %). It is notable that, in both cases, the winds were from the north-northwest and the wind speed increased considerably from less than $1\,m\,s^{-1}$ to $3.1\,m\,s^{-1}$ during the particle shrinkage. Additionally, the SO_2 increased substantially along with the increased wind speed; however, it did not result in another intense NPF, as did on the 12 and 17 August 2010. The particle shrinkage at the downwind site differs from others mainly in the early termination of particle shrinkage. In comparison to other shrinkage events, such difference may arise due to a couple of reasons. First, the chemical constituents of the new particles at the downwind site may be different and less volatile than the other sites. Second, the atmospheric dilution during the shrinkage at the downwind site was relatively poorer, which is evident by the lower mixing height (max. 460–470 m) and hence higher CS (max. $3.6–4.0 \times 10^{-2}\,s^{-1}$). Under polluted air, the concentrations of condensable vapor are presumably higher. As a result, the evaporation of semi-volatile species is more limited.

ACPD
12, 18605–18650, 2012

3.6.4 Candidate evaporating vapors

At present it is unclear what were the evaporating vapors involved during the particle shrinkage. Potential candidates include semi-volatile ammonium nitrate (NH_4NO_3) and organics compounds such as *n*-alkanes and polycyclic aromatic hydrocarbons (PAHs) due to their high volatility. At the same urban site of this study, Cheng and Tsai (2000) showed that, in addition to elemental carbon and sulfate (SO_4^{2-}), the major resolved chemical constituents in $PM_{2.5}$ were organic carbon, followed by NH_4^+ and NO_3^-. Their respective average concentrations were about 15 $\mu g\,m^{-3}$, 4 $\mu g\,m^{-3}$ and 4 $\mu g\,m^{-3}$, respectively. In addition, they showed that the NO_3^- and carbonaceous contents in the urban area were approximately 1.5–2 times higher than that in the coastal area. In Central Taiwan, Fang et al. (2006) showed that the major ionic species in ultrafine particles were SO_4^{2-}, followed by NH_4^+ and NO_3^-. Furthermore Lin et al. (2006) reported the annual average of NH_3 was 12.3 ppb, with the highest average of 16.4 ppb observed in the summer. More recently, Bzdek et al. (2012) showed that 29–46 % of the total mass growth of new particles were attributable to SO_4^{2-} at an urban site in Wilmington, DE, USA. The remaining, more than 50 %, new particle growth was due to NO_3^-, NH_4^+ and organics. The above studies demonstrate the potentially abundant and semi-volatile NH_4^+, NO_3^- and organics in the particle phase, and thus suggest that they may have involved in the particle shrinkage in the present study. We also do not exclude the possible involvement of organic compounds such as organic acids and amines, but there were no chemical analysis made at our observation sites to support our hypothesis.

4 Conclusions

This study provides the first systematic analysis for new particle formation (NPF) and growth events at four distinct types of environment (urban, coastal, mountain and downwind) in an air quality management district of subtropical Central Taiwan. A total of 14 NPF and growth events were identified from October 2008 to January 2009 and from

ACPD
12, 18605–18650, 2012

August 2010 to October 2010, classified with respect to their start times (t_{start}) and analyzed for aerosol characteristics, air pollutant and meteorological conditions. Accordingly, there were nine type A events with t_{start} before 09:00 LT and five type B events with t_{start} after 09:00 LT. Type A events were preferred on days that started off with low condensation sink (CS), and coincided with periods with increased morning traffic emissions and the breakup of nocturnal inversion layer. It is possible that SO_2 and H_2SO_4 were also involved in traffic-related ultrafine particles (type A). Nevertheless, the lower or comparable SO_2 on event days than on non-event days suggests that SO_2 was not a limiting factor for NPF. In particular, the strong connection between the start of type A events and traffic rush hours suggests that traffic emissions likely contain certain nucleating and condensable vapors. On the other hand, type B events were preferred on days that started off with high CS and coincided with enhanced atmospheric dilution and dispersion after 09:00 LT until the midday. In addition, type B events were preferred during periods with minimum levels of primary traffic emissions. The type B events were preferred on days that involve intense midday atmospheric dilution, which appears to be a necessary factor because of the elevated pre-existing particles prior to events.

It is notable that all 11 NPF events took place in the warm season (August to October) (nine of them are type A events) and nine events occurred at the urban site (eight of them are type A events). These preferences are consistent with the fact that the warm season in Taiwan in general is characterized lower PM pollution and stronger solar radiation, and the urban site is also characterized by elevated traffic emissions. Overall, NPF events contributed significantly to the ambient ultrafine particles, with the maximum concentrations of 2.5–8.9 $\times$ 10^4 cm^{-3} 2–4 times higher than that due to typical traffic emissions. The nucleation rates J_1 and growth rates GR_{PARGAN} inverted from the measured aerosol size distributions were in the range of 39.6–252.9 $cm^{-3}\,s^{-1}$ and 6.5–14.5 $nm\,h^{-1}$, respectively. The approximation derived J_{10} and growth rates GR_{MOD} were in the range of 4.4–29.8 $cm^{-3}\,s^{-1}$ and 7.4–23.9 $nm\,h^{-1}$, respectively.

ACPD
12, 18605–18650, 2012

A unique feature of our observations in the present study is particle shrinkage. There were five shrinkage events out of 14 NPF events. Their respective GR_{MOD} ranged from -5.1 to $-7.6\,nm\,h^{-1}$. The ratios of shrinkage-to-growth rates were mostly in the range of 0.40–0.65, suggesting significant contributions of semi-volatile species to the new particle growth. In intense cases where particles shrank back to the smallest measurable size of $\sim 10\,nm$, the new particle growth and shrinkage thereby created a unique "arch-like" shape in the size distribution contour plot. Time-series analyses of air pollutants and meteorological conditions indicate that the particle shrinkage was related to air masses with low CS due to atmospheric dilution, high ambient temperature and low relative humidity. Such atmospheric conditions favor the evaporation of semi-volatile species from the particle phase to the gas phase. Although chemical identification of the potential evaporating vapors was not possible in the present study we speculate that the candidate vapors can be semi-volatile NH_4^+, NO_3^- and organics such as *n*-alkanes and PAHs due to their high volatility and abundance in the study area. Chemical analysis of the nucleating and condensing/evaporating vapors is required to infer more definitive mechanisms of NPF, particle growth and shrinkage that are relevant to climate change and public health.

A1 Eight consecutive type A NPF events with two particle shrinkage events

Figure A1 shows the diurnal variations of the number size distributions during eight consecutive type A NPF events at the urban site from the 10 to the 17 August 2010. Among them there were two particle shrinkage events on the 12 and the 16 August 2010. As shown, the particles initially grew to sizes of 50–60 nm and then shrank back to the smallest measurable sizes of $\sim 10\,nm$, creating a unique "arch-like" shape in the contour plot.

ACPD
12, 18605–18650, 2012

A2 Regional-scale SO_2 impact

Figure A2 shows the diurnal variations of SO_2 at the present urban site (JM) and three nearby air quality monitoring sites on the 12 August 2010. The regional-scale SO_2 impact occurred at 15:00 LT.

Acknowledgements. The authors wish to express their appreciation to the Taiwan EPA for making the air quality monitoring sites available for the present study. The financial support from the Taiwan National Science Council (NSC97-2218-E-039-002-MY3 and NSC100-2628-E-039-001-MY3) and the China Medical University (CMU98-N1-26) are gratefully acknowledged.

References

Anttila, T., Kerminen, V.-M., and Lehtinen, K. E. J.: Parameterizing the formation rate of new particles the effect of nuclei self-coagulation, J. Aerosol Sci., 41, 621–636, 2010.

Atkinson, R. W., Fuller, G. W., Anderson, H. R., Harrison, R. M., and Armstrong, B.: Urban ambient particle metrics and health, Epidemiology, 21, 501–511, 2010.

Backman, J., Rizzo, L. V., Hakala, J., Nieminen, T., Manninen, H. E., Morais, F., Aalto, P. P., Siivola, E., Carbone, S., Hillamo, R., Artaxo, P., Petäjä, T., and Kulmala, M.: The variability of urban aerosol size distributions and optical properties in São Paulo – Brazil: new particle formation events occur at the site, Atmos. Chem. Phys. Discuss., 11, 30419–30455, doi:10.5194/acpd-11-30419-2011, 2011.

Baron, P. A. and Willeke, K.: Aerosol Measurement: Principles, Techniques, and Applications, second ed., John Wiley and Sons, New York, 2001.

Benson, D. R., Yu, J. H., Markovich, A., and Lee, S.-H.: Ternary homogeneous nucleation of H_2SO_4, NH_3, and H_2O under conditions relevant to the lower troposphere, Atmos. Chem. Phys., 11, 4755–4766, doi:10.5194/acp-11-4755-2011, 2011.

Boy, M. and Kulmala, M.: Nucleation events in the continental boundary layer: Influence of physical and meteorological parameters, Atmos. Chem. Phys., 2, 1–16, doi:10.5194/acp-2-1-2002, 2002.

ACPD
12, 18605–18650, 2012

Bzdek, B. R. and Johnston, M. V.: New particle formation and growth in the troposphere, Anal. Chem., 82, 7871–7878, 2010.
Bzdek, B. R., Zordan, C. A., Pennington, M. R., Luther, G. W., III, and Johnston, M. V.: Quantitative assessment of the sulfuric acid contribution to new particle growth, Environ. Sci. Technol., 46, 4365–4373, doi:10.1021/es204556c, 2012.
Cheng, M. T. and Tsai, Y. I.: Characterization of visibility and atmospheric aerosols in urban, suburban, and remote areas, Sci. Total Environ., 263, 101–114, 2000.
Dal Maso, M., Kulmala, M., Riipinen, I., Wagner, R., Hussein, T., Aalto, P. P., and Lehtinen, K. E. J.: Formation and growth of fresh atmospheric aerosols: eight years of aerosol size distribution data from SMEAR II, Hyytiälä, Finland, Boreal Environ. Res., 10, 323–336, 2005.
Erupe, M. E., Benson, D. R., Li, J., Young, L.-H., Verheggen, B., Al-Refai, M., Tahboub, O., Cunningham, V., Frimpong, F., Viggiano, A. A., and Lee, S.-H.: Correlation of aerosol nucleation rate with sulfuric acid and ammonia in Kent, Ohio: an atmospheric observation, J. Geophys. Res., 115, D23216, doi:10.1029/2010JD013942, 2010.
Erupe, M. E., Viggiano, A. A., and Lee, S.-H.: The effect of trimethylamine on atmospheric nucleation involving H_2SO_4, Atmos. Chem. Phys., 11, 4767–4775, doi:10.5194/acp-11-4767-2011, 2011.
Fang, G.-C., Wu, Y.-S., Chang, S.-Y., Rau, J.-Y., Huang, S.-H., and Lin, C.-K.: Characteristic study of ionic species in nano, ultrafine, fine and coarse particle size mode at a traffic sampling site, Toxicol. Ind. Health, 22, 27–37, 2006.
Fuchs, N. A. and Sutugin, A. G.: Highly Dispersed Aerosols, Pergamon, New York, USA, 1971.
Gurjar, B., Butler, T., Lawrence, M., and Lelieveld, J.: Evaluation of emissions and air quality in megacities, Atmos. Environ., 42, 1593–1606, 2008.
Hallar, A., Lowenthal, D. H., Chirokova, G., Borys, R. D., and Wiedinmyer, C.: Persistent daily new particle formation at a mountain-top location, Atmos. Environ., 45, 4111–4115, 2011.
Hegg, D. A. and Baker, M. B.: Nucleation in the atmosphere, Rep. Prog. Phys., 72, 056801, doi:10.1088/0034-4885/72/5/056801, 2009.
Heikkilä, J., Virtanen, A., Rönkkö, T., Keskinen, J., Aakko-Saksa, P., and Murtonen, T.: Nanoparticle emissions from a heavy-duty engine running on alternative diesel fuels, Environ. Sci. Technol., 43, 9501–9506, 2009.
Heim, M., Kasper, G., Reischl, G. P., and Gerhart, C.: Performance of a new commercial electrical mobility spectrometer, Aerosol Sci. Technol., 38, 3–14, 2004.

ACPD
12, 18605–18650, 2012

Holmes, N. S.: A review of particle formation events and growth in the atmosphere in the various environments and discussion of mechanistic implications, Atmos. Environ., 41, 2183–2201, 2007.
Iida, K., Stolzenburg, M., and McMurry, P.: Estimating nanoparticle growth rates from size-dependent charged fractions: analysis of new particle formation events in Mexico City, J. Geophys. Res., 113, D05207, doi:10.1029/2007JD009260, 2008.
Jacobson, M. Z., Kittelson, D. B., and Watts, W. F.: Enhanced coagulation due to evaporation and its effect on nanoparticle evolution, Environ. Sci. Technol., 39, 9486–9492, 2005.
Kanawade, V. P., Benson, D. R., and Lee, S.-H.: Statistical analysis of 4-year observations of aerosol sizes in a semi-rural continental environment, Atmos. Environ., 59, 30–38, 2012.
Kerminen, V.-M., Petäjä, T., Manninen, H. E., Paasonen, P., Nieminen, T., Sipilä, M., Junninen, H., Ehn, M., Gagné, S., Laakso, L., Riipinen, I., Vehkamäki, H., Kurten, T., Ortega, I. K., Dal Maso, M., Brus, D., Hyvärinen, A., Lihavainen, H., Leppä, J., Lehtinen, K. E. J., Mirme, A., Mirme, S., Hõrrak, U., Berndt, T., Stratmann, F., Birmili, W., Wiedensohler, A., Metzger, A., Dommen, J., Baltensperger, U., Kiendler-Scharr, A., Mentel, T. F., Wildt, J., Winkler, P. M., Wagner, P. E., Petzold, A., Minikin, A., Plass-Dülmer, C., Pöschl, U., Laaksonen, A., and Kulmala, M.: Atmospheric nucleation: highlights of the EUCAARI project and future directions, Atmos. Chem. Phys., 10, 10829–10848, doi:10.5194/acp-10-10829-2010, 2010.
Kroll, J. H., Ng, N. L., Murphy, S. M., Flagan, R. C., and Seinfeld, J. H.: Secondary organic aerosol formation from isoprene photooxidation, Environ. Sci. Technol., 40, 1869–1877, 2006.
Kuang, C., McMurry, P. H., McCormick, A. V., and Eisele, F. L.: Dependence of nucleation rates on sulfuric acid vapor concentration in diverse atmospheric locations, J. Geophys. Res., 113, D10209, doi:10.1029/2007JD009253, 2008.
Kulmala, M.: How particles nucleate and grow, Science, 302, 1000–1001, 2003.
Kulmala, M. and Kerminen, V. M.: On the formation and growth of atmospheric nanoparticles, Atmos. Res., 90, 132–150, 2008.
Kulmala, M., Vehkamaki, H., Petaja, T., Dal Maso, M., Lauri, A., Kerminen, V., Birmili, W., and McMurry, P.: Formation and growth rates of ultrafine atmospheric particles: a review of observations, J. Aerosol Sci., 35, 143–176, 2004.
Laaksonen, A., Kulmala, M., O'Dowd, C. D., Joutsensaari, J., Vaattovaara, P., Mikkonen, S., Lehtinen, K. E. J., Sogacheva, L., Dal Maso, M., Aalto, P., Petäjä, T., Sogachev, A., Yoon, Y. J., Lihavainen, H., Nilsson, D., Facchini, M. C., Cavalli, F., Fuzzi, S., Hoffmann, T., Arnold, F.,

ACPD
12, 18605–18650, 2012

Hanke, M., Sellegri, K., Umann, B., Junkermann, W., Coe, H., Allan, J. D., Alfarra, M. R., Worsnop, D. R., Riekkola, M.-L., Hyötyläinen, T., and Viisanen, Y.: The role of VOC oxidation products in continental new particle formation, Atmos. Chem. Phys., 8, 2657–2665, doi:10.5194/acp-8-2657-2008, 2008.

Lehtinen, K. E. J., Dal Maso, M., Kulmala, M., and Kerminen, V.-M.: Estimating nucleation rates from apparent particle formation rates and vice versa: revised formulation of the Kerminen-Kulmala equation, J. Aerosol Sci., 38, 988–994, 2007.

Lin, Y. C., Cheng, M. T., Ting, W. Y., and Yeh, C. R.: Characteristics of gaseous HNO_2, HNO_3, NH_3 and particulate ammonium nitrate in an urban city of Central Taiwan, Atmos. Environ., 40, 4725–4733, 2006.

Lyman, W. J., Reehl, W. F., and Rosenblatt, D. H.: Handbook of Chemical Property Estimation Methods, American Chemical Society, Washington DC, USA, 1990.

Merikanto, J., Spracklen, D. V., Mann, G. W., Pickering, S. J., and Carslaw, K. S.: Impact of nucleation on global CCN, Atmos. Chem. Phys., 9, 8601–8616, doi:10.5194/acp-9-8601-2009, 2009.

Metzger, A., Verheggen, B., Dommen, J., Duplissy, J., Prevot, A. S. H., Weingartner, E., Riipinen, I., Kulmala, M., Spracklen, D. V., and Carslaw, K. S.: Evidence for the role of organics in aerosol particle formation under atmospheric conditions, Proc. Nat. Acad. Sci. USA, 107, 6646–6651, 2010.

Molina, M. J.: Atmospheric evolution of organic aerosol, Geophys. Res. Lett., 31, L22104, doi:10.1029/2004GL020910, 2004.

Morawska, L., Ristovski, Z., Jayaratne, E. R., Keogh, D. U., and Ling, X.: Ambient nano and ultrafine particles from motor vehicle emissions: characteristics, ambient processing and implications on human exposure, Atmos. Environ., 42, 8113–8138, 2008.

Mönkkönen, P., Koponen, I. K., Lehtinen, K. E. J., Hameri, K., Uma, R., and Kulmala, M.: Measurements in a highly polluted Asian mega city: observations of aerosol number size distribution, modal parameters and nucleation events, Atmos. Chem. Phys., 5, 57–66, doi:10.5194/acp-5-57-2005, 2005.

Nel, A.: Toxic potential of materials at the nanolevel, Science, 311, 622–627, 2006.

Peng, R. D., Bell, M. L., Geyh, A. S., McDermott, A., Zeger, S. L., Samet, J. M., and Dominici, F.: Emergency admissions for cardiovascular and respiratory diseases and the chemical composition of fine particle air pollution, Environ. Health Persp., 117, 957–963, 2009.

ACPD
12, 18605–18650, 2012

Pierce, J. R., Leaitch, W. R., Liggio, J., Westervelt, D. M., Wainwright, C. D., Abbatt, J. P. D., Ahlm, L., Al-Basheer, W., Cziczo, D. J., Hayden, K. L., Lee, A. K. Y., Li, S.-M., Russell, L. M., Sjostedt, S. J., Strawbridge, K. B., Travis, M., Vlasenko, A., Wentzell, J. J. B., Wiebe, H. A., Wong, J. P. S., and Macdonald, A. M.: Nucleation and condensational growth to CCN sizes during a sustained pristine biogenic SOA event in a forested mountain valley, Atmos. Chem. Phys., 12, 3147–3163, doi:10.5194/acp-12-3147-2012, 2012.

Pirjola, L., O'Dowd, C. D., and Kulmala, M.: A model prediction of the yield of cloud condensation nuclei from coastal nucleation events, J. Geophys. Res., 107, 8098, 10.1029/2000JD000213, 2002.

Raga, G., Baumgardner, D., Castro, T., Martinez-Arroyo, A., and Navarro-González, R.: Mexico City air quality: a qualitative review of gas and aerosol measurements (1960–2000), Atmos. Environ., 35, 4041–4058, 2001.

Riipinen, I., Pierce, J. R., Yli-Juuti, T., Nieminen, T., Häkkinen, S., Ehn, M., Junninen, H., Lehtipalo, K., Petäjä, T., Slowik, J., Chang, R., Shantz, N. C., Abbatt, J., Leaitch, W. R., Kerminen, V.-M., Worsnop, D. R., Pandis, S. N., Donahue, N. M., and Kulmala, M.: Organic condensation: a vital link connecting aerosol formation to cloud condensation nuclei (CCN) concentrations, Atmos. Chem. Phys., 11, 3865–3878, doi:10.5194/acp-11-3865-2011, 2011.

Salma, I., Borsós, T., Weidinger, T., Aalto, P., Hussein, T., Dal Maso, M., and Kulmala, M.: Production, growth and properties of ultrafine atmospheric aerosol particles in an urban environment, Atmos. Chem. Phys., 11, 1339–1353, doi:10.5194/acp-11-1339-2011, 2011.

Seinfeld, J. H. and Pandis, S. N.: Atmospheric Chemistry and Physics, 2nd Edn., John Wiley and Sons, New York, 2006.

Shen, X. J., Sun, J. Y., Zhang, Y. M., Wehner, B., Nowak, A., Tuch, T., Zhang, X. C., Wang, T. T., Zhou, H. G., Zhang, X. L., Dong, F., Birmili, W., and Wiedensohler, A.: First long-term study of particle number size distributions and new particle formation events of regional aerosol in the North China Plain, Atmos. Chem. Phys., 11, 1565–1580, doi:10.5194/acp-11-1565-2011, 2011.

Sipila, M., Berndt, T., Petaja, T., Brus, D., Vanhanen, J., Stratmann, F., Patokoski, J., Mauldin, R. L., Hyvarinen, A. P., Lihavainen, H., and Kulmala, M.: The role of sulfuric acid in atmospheric nucleation, Science, 327, 1243–1246, 2010.

Smith, J. N., Barsanti, K. C., Friedli, H. R., Ehn, M., Kulmala, M., Collins, D. R., Scheckman, J. H., Williams, B. J. and McMurry, P. H.: Observations of aminium salts in atmospheric

ACPD
12, 18605–18650, 2012

nanoparticles and possible climatic implications, Proc. Nat. Acad. Sci. USA, 107, 6634–6639, 2010.
Stanier, C. O., Khlystov, A. Y., and Pandis, S. N.: Nucleation Events during the Pittsburgh air quality study: description and relation to key meteorological, gas phase, and aerosol parameters, Aerosol Sci. Technol., 38, 253–264, 2004.
Stolzenburg, M. R., McMurry, P. H., Sakurai, H., Smith, J. N., Mauldin, R. L., III, Eisele, F. L., and Clement, C. F.: Growth rates of freshly nucleated atmospheric particles in Atlanta, J. Geophys. Res., 110, D22S05, doi:10.1029/2005JD005935, 2005.
TW EPA: Air Quality Annual Report of R.O.C (Taiwan), Taiwan Environmental Protection Administration, Taipei, Taiwan, 2009.
Verheggen, B. and Mozurkewich, M.: An inverse modeling procedure to determine particle growth and nucleation rates from measured aerosol size distributions, Atmos. Chem. Phys., 6, 2927–2942, doi:10.5194/acp-6-2927-2006, 2006.
Wu, Z., Hu, M., Liu, S., Wehner, B., Bauer, S., Maßling, A., Wiedensohler, A., Petäjä, T., Dal Maso, M., and Kulmala, M.: New particle formation in Beijing, China: statistical analysis of a 1-year data set, J. Geophys. Res., 112, D09209, doi:10.1029/2006JD007406, 2007.
Yao, X., Choi, M. Y., Lau, N. T., Lau, A. P. S., Chan, C. K., and Fang, M.: Growth and shrinkage of new particles in the atmosphere in Hong Kong, Aerosol Sci. Technol., 44, 639–650, 2010.
Young, L.-H., Liou, Y.-J., Cheng, M.-T., Lu, J.-H., Yang, H.-H., Tsai, Y. I., Wang, L.-C., Chen, C.-B., and Lai, J.-S.: Effects of biodiesel, engine load and diesel particulate filter on nonvolatile particle number size distributions in heavy-duty diesel engine exhaust, J. Hazard. Mater., 199–200, 282–289, 2012a.
Young, L.-H., Wang, Y.-T., Hsu, H.-C., Lin, C.-H., Liou, Y.-J., Lai, Y.-C., Lin, Y.-H., Chang, W.-L., Chiang, H.-L., and Cheng, M.-T.: Spatiotemporal variability of submicrometer particle number size distributions in an air quality management district, Sci. Total Environ., 425, 135–145, 2012b.
Yu, H., McGraw, R., and Lee, S.-H.: Effects of amines on formation of sub-3 nm particles and their subsequent growth, Geophys. Res. Lett., 39, L02807, doi:10.1029/2011GL050099, 2012.
Yue, D. L., Hu, M., Zhang, R. Y., Wang, Z. B., Zheng, J., Wu, Z. J., Wiedensohler, A., He, L. Y., Huang, X. F. and Zhu, T.: The roles of sulfuric acid in new particle formation and growth in the mega-city of Beijing, Atmos. Chem. Phys., 10, 4953–4960, doi:10.5194/acp-10-4953-2010, 2010.

ACPD
12, 18605–18650, 2012

Zanobetti, A. and Schwartz, J.: The effect of fine and coarse particulate air pollution on mortality: a national analysis, Environ. Health Persp., 117, 898–903, 2009.
Zhang, K. M. and Wexler, A. S.: A hypothesis for growth of fresh atmospheric nuclei, J. Geophys. Res., 107, 4577 doi:10.1029/2002JD002180, 2002.
Zhang, K. M. and Wexler, A. S.: Evolution of particle number distribution near roadways – Part I: Analysis of aerosol dynamics and its implications for engine emission measurement, Atmos. Environ., 38, 6643–6653, 2004.
Zhang, R., Suh, I., Zhao, J., Zhang, D., Fortner, E. C., Tie, X., Molina, L. T. and Molina, M. J.: Atmospheric new particle formation enhanced by organic acids, Science, 304, 1487–1490, 2004.
Zhang, R., Wang, L., Khalizov, A. F., Zhao, J., Zheng, J., McGraw, R. L., and Molina, L. T.: Formation of nanoparticles of blue haze enhanced by anthropogenic pollution, Proc. Nat. Acad. Sci. USA, 106, 17650–17654, 2009.
Zhang, R., Khalizov, A., Wang, L., Hu, M., and Xu, W.: Nucleation and growth of nanoparticles in the atmosphere, Chem. Rev., 112, 1957–2011, 2012.

ACPD
12, 18605–18650, 2012

Table 1. NPF event types, growth durations, daily meteorological conditions and air pollutant concentrations at the urban, coastal and downwind sites. T indicates temperature and CS condensation sink. Daily averages of T, RH, wind speed, $PM_{2.5}$, CS and SO_2 are shown here.

Date	Site[1]	Day of the Week	Type[2]	NPF start/end time t_{start}	t_{end}	Δt[3]	T (°C)	RH (%)	Wind Speed (m s^{-1})	WindDirection Direction	$PM_{2.5}$ (μg m^{-3})	CS (10^{-2} s^{-1})	SO_2 (ppb)
3 Dec 2008	D	Wed.	B	10:18	15:03	4:44	18.0	66.5	0.6	E	46.6	3.9	3.4
17 Dec 2008	U	Wed.	B	12:02	13:57	1:55	18.4	59.3	0.5	N, NE	40.4	3.2	3.3
3 Jan 2009	C	Sat.	B-S	10:31	13:26	2:55	16.0	63.8	3.4	N	19.4	2.2	3.7
10 Aug 2010	U	Tue.	A	8:17	13:11	4:54	31.7	69.3	1.9	S, SW	17.9	2.1	3.5
11 Aug 2010	U	Wed.	A	7:37	11:56	4:19	30.3	76.5	1.3	S	15.8	2.4	2.8
12 Aug 2010	U	Thu.	A-S	8:07	12:26	4:19	30.0	74.0	1.2	S, SE	18.9	2.0	2.6
13 Aug 2010	U	Fri.	A	7:13	12:14	5:00	30.2	71.4	1.2	S, W	17.0	1.9	2.1
14 Aug 2010	U	Sat.	A	8:59	13:32	4:33	30.6	72.1	1.2	S, W	17.0	2.2	2.3
15 Aug 2010	U	Sun.	A	8:54	10:32	1:38	29.6	71.0	1.0	S, SE	16.5	2.0	2.0
16 Aug 2010	U	Mon.	A-S	8:28	11:09	2:41	30.0	70.3	1.2	S	17.0	2.2	–
17 Aug 2010	U	Tue.	A	9:05	12:35	3:30	29.5	71.8	0.7	SE	19.0	2.6	4.6
5 Sep 2010	D	Sun.	B-S	9:40	11:53	2:13	27.0	83.1	1.1	NW, SW	15.5	1.7	2.1
7 Sep 2010	D	Tue.	B-S	10:07	12:41	2:34	27.5	81.5	1.1	SW, NW	26.4	2.0	2.4
12 Sep 2010	D	Sun.	A	9:07	13:26	4:19	25.8	84.3	0.9	W	10.1	1.6	2.9

[1]U indicates urban, C coastal, and D downwind sites. There were no NPF events observed at the mountain site. The same for Table 2.
[2]Type A and B refer to events with start time (t_{start}) before and after ~ 09:00 and thus with and without influences from traffic. Ones followed by "-S" indicate particle shrinkage. The same for Table 2.
[3]The duration between the t_{start} to end of particle growth (t_{end}).

ACPD
12, 18605–18650, 2012

Table 2. Size-segregated particle number concentrations, nucleation and growth rates during the NPF events.

Date	Site	Type	Number Conc.* (10^4 cm^{-3}) N_{10-25}	N_{25-100}	Nucleation/Formation Rate (cm^{-3} s^{-1}) J_1	J_{10}	Growth Rate (nm h^{-1}) GR_{PARGAN}	GR_{MOD}	GR_{MOD}
3 Dec 2008	D	B	2.0	1.3	113.1	14.5	6.7	7.4	–
17 Dec 2008	U	B	1.7	1.4	182.3	7.0	6.6	23.9	–
3 Jan 2009	C	B-S	2.2	1.7	98.8	7.2	14.5	7.8	−5.1
10 Aug 2010	U	A	3.3	2.5	195.2	15.6	8.5	14.5	–
11 Aug 2010	U	A	3.9	2.5	252.9	29.8	7.2	9.3	–
12 Aug 2010	U	A-S	3.0	2.5	216.3	16.2	7.4	10.7	−5.6
13 Aug 2010	U	A	3.5	2.9	208.9	18.3	9.1	6.7	–
14 Aug 2010	U	A	2.9	3.0	202.9	24.7	6.5	12.8	–
15 Aug 2010	U	A	4.0	3.2	172.2	26.5	8.4	7.6	–
16 Aug 2010	U	A-S	3.9	3.3	188.0	22.5	9.5	17.3	−6.9
17 Aug 2010	U	A	2.9	2.9	131.9	21.8	8.2	12.8	–
5 Sep 2010	D	B-S	1.4	2.4	39.6	4.4	12.2	15.4	−7.1
7 Sep 2010	D	B-S	1.6	1.5	82.1	8.4	7.8	7.4	−7.6
12 Sep 2010	D	A	1.2	2.2	65.3	10.6	9.6	10.9	–

*The average concentrations from the start of NPF to the end of particle growth.

ACPD
12, 18605–18650, 2012

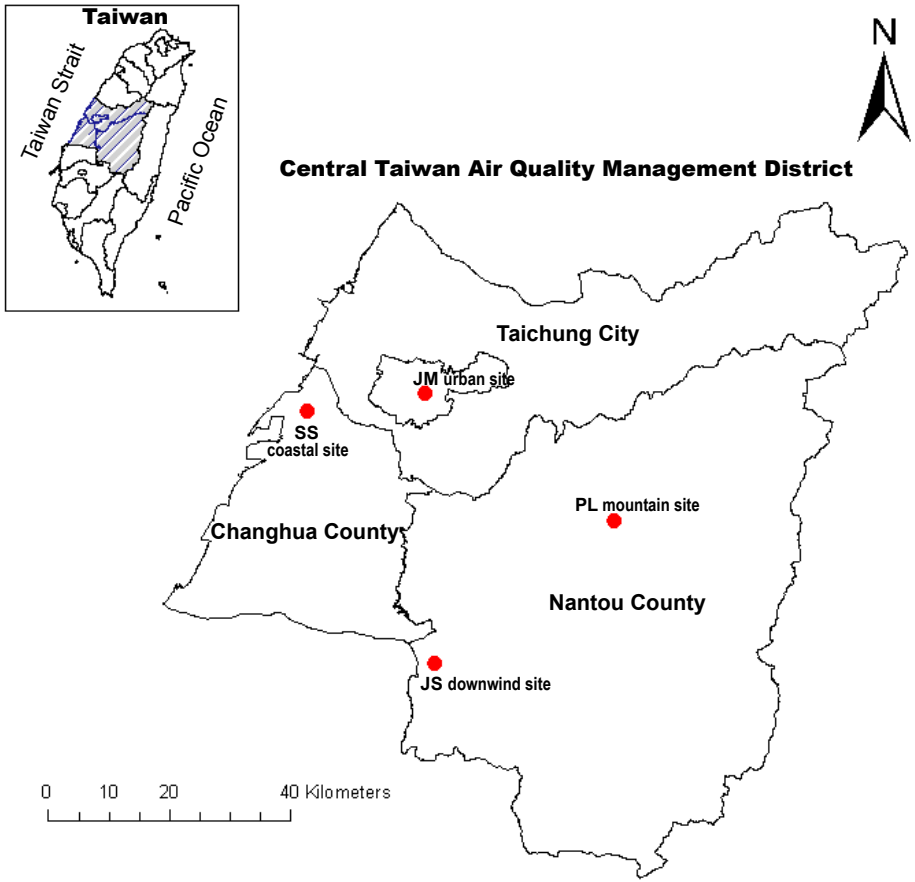

Fig. 1. Map of the four observation sites in the Central Taiwan air quality management district.

ACPD
12, 18605–18650, 2012

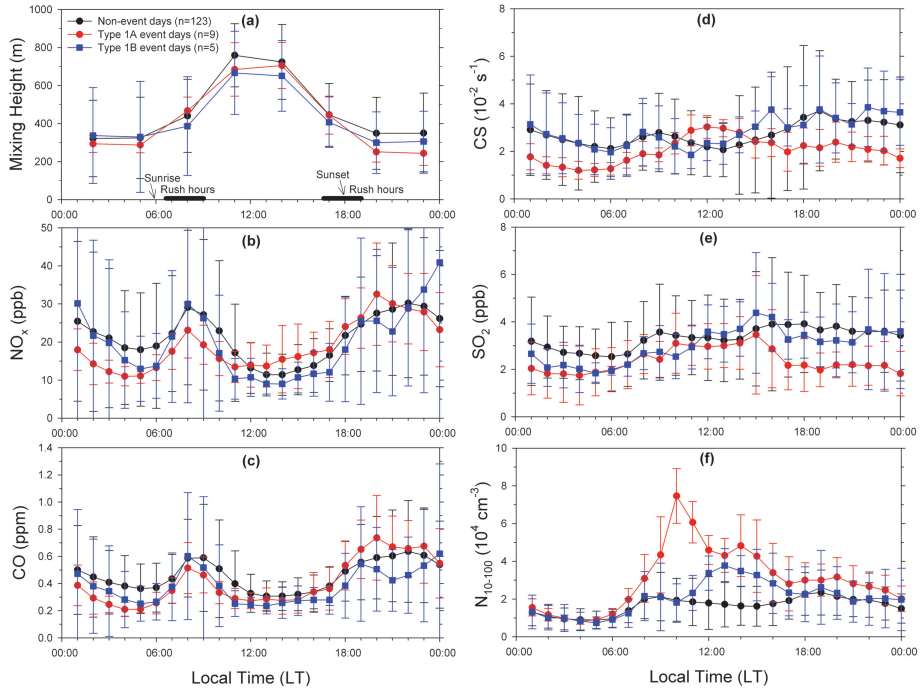

Fig. 2. Diurnal variations of the average **(a)** mixing height, **(b)** NO_x **(c)** CO, **(d)** condensation sink (CS), **(e)** SO_2 and **(f)** 10–100 nm particle number (N_{10-100}) concentrations on non-event, type A and type B event days. In the SO_2 plot, one type A event seen on the 17 August 2008 was excluded because of the exceptionally high SO_2 (17 ppb) at 15:00 LT.

ACPD
12, 18605–18650, 2012

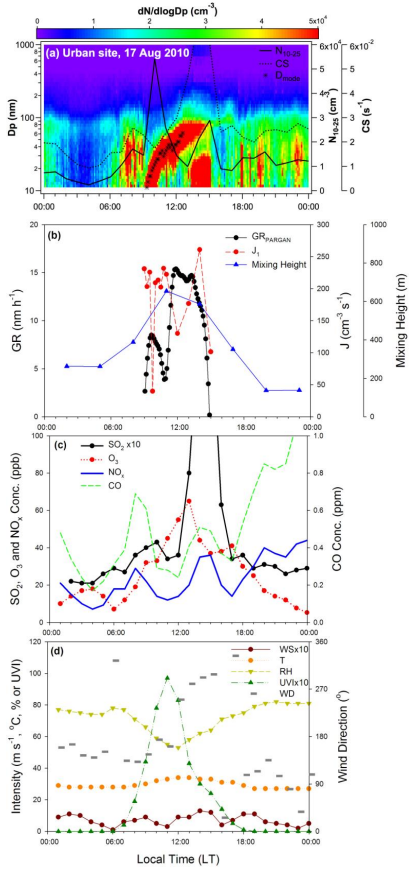

Fig. 3. The evolution of **(a)** the number size distributions, N_{10-25}, CS and particle mode diameter (D_{mode}), **(b)** the GR_{PARGAN}, J_1 and mixing height, **(c)** the hourly SO_2, O_3, NO_x and CO, and **(d)** the meteorological conditions (WS, T, RH, WD and UVI) during a type A NPF and growth event on the 17 August 2010.

ACPD
12, 18605–18650, 2012

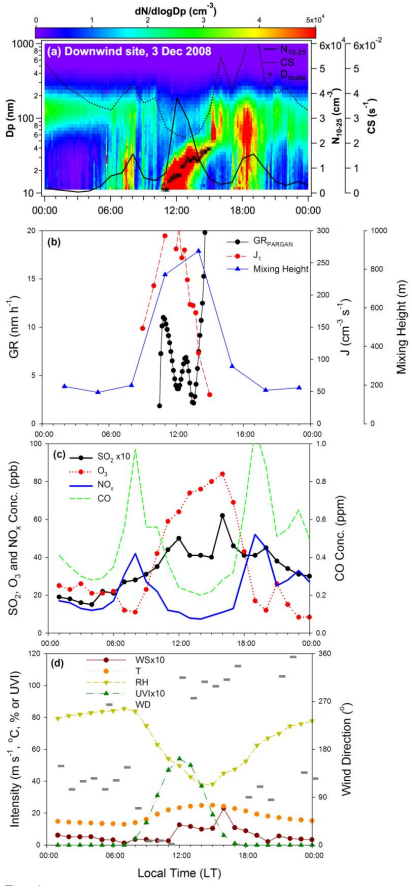

Fig. 4. The same as Fig. 3, except this is for during a type B NPF and growth event on the 3 December 2008.

ACPD
12, 18605–18650, 2012

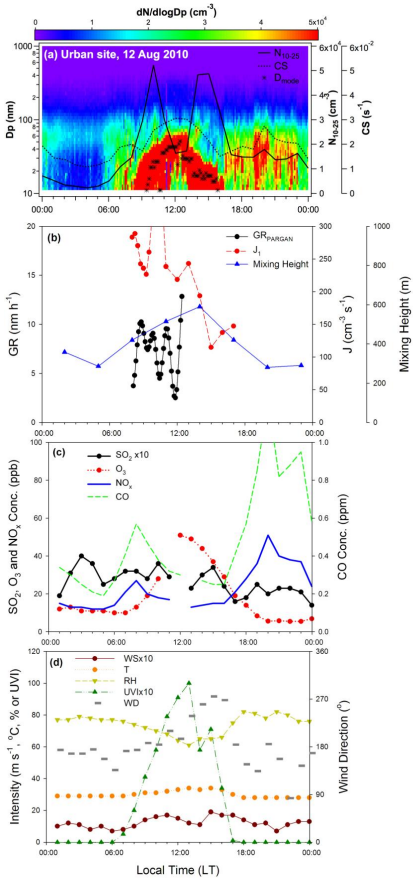

Fig. 5. The same as Fig. 3, except this is for during a type A-S NPF, growth and shrinkage event on the 12 August 2010.

ACPD
12, 18605–18650, 2012

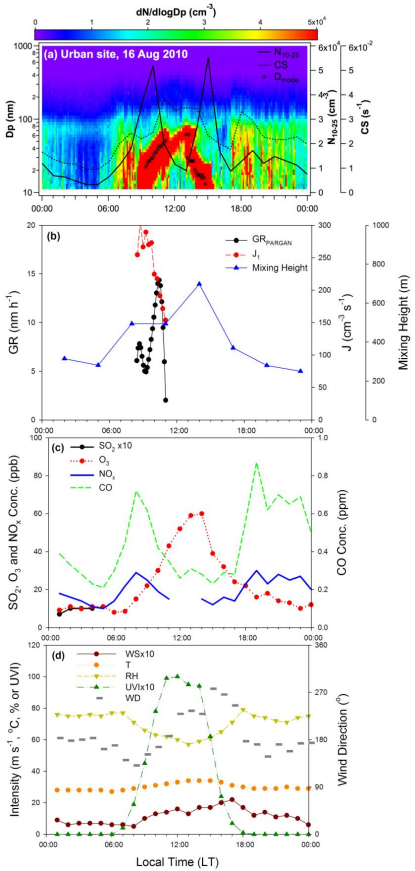

Fig. 6. The same as Fig. 3, except this is for during a type A-S NPF, growth and shrinkage event on the 16 August 2010.

ACPD
12, 18605–18650, 2012

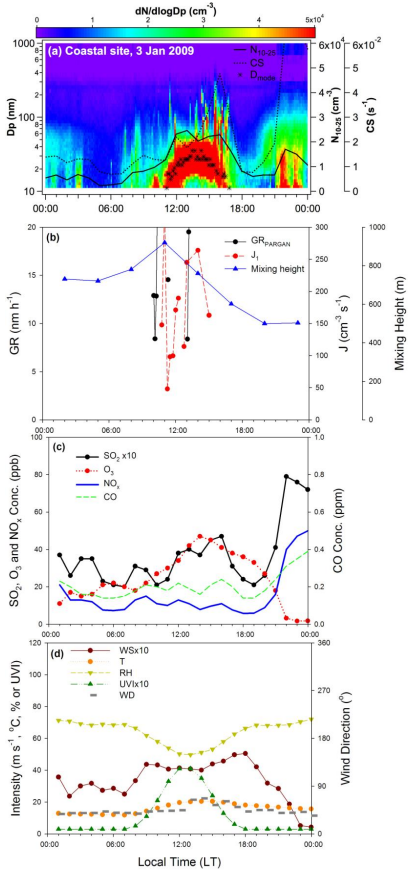

Fig. 7. The same as Fig. 3, except this is for during a type B-S NPF, growth and shrinkage event on the 3 January 2009.

ACPD
12, 18605–18650, 2012

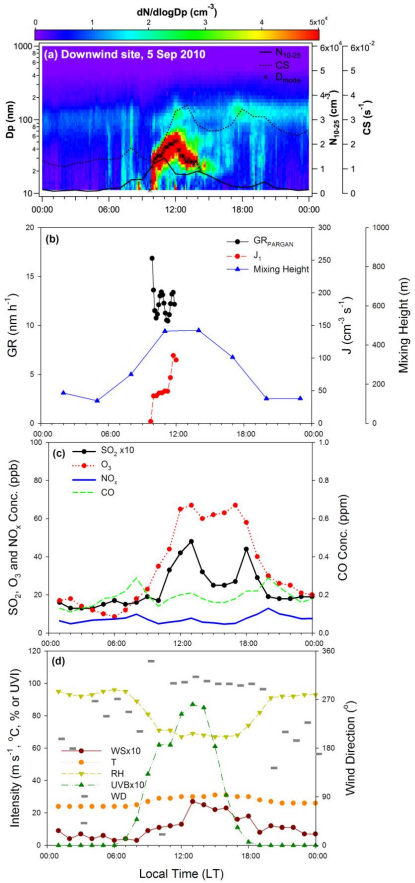

Fig. 8. The same as Fig. 3, except this is for during a type B-S NPF, growth and shrinkage event on the 5 September 2010.

ACPD
12, 18605–18650, 2012

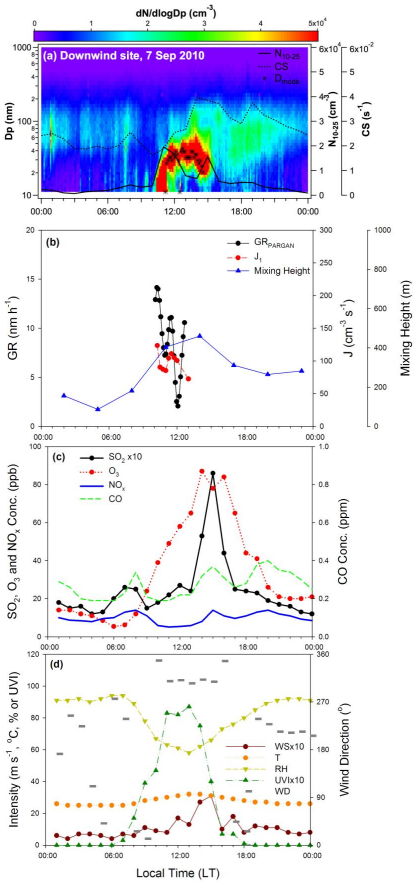

Fig. 9. The same as Fig. 3, except this is for during a type B-S NPF, growth and shrinkage event on the 7 September 2010.

ACPD
12, 18605–18650, 2012

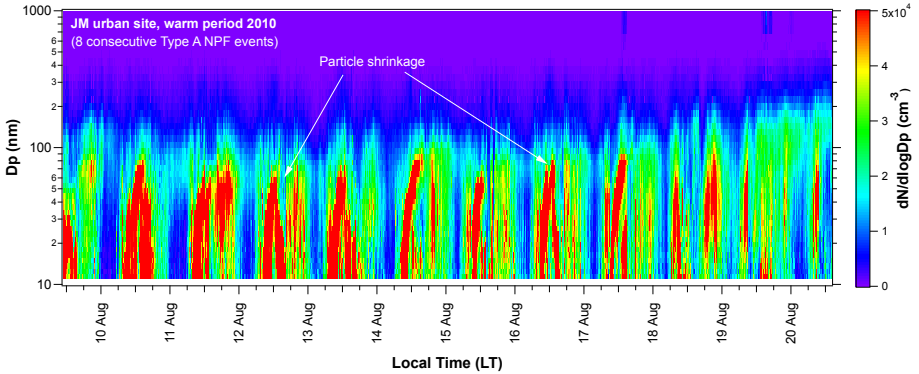

Fig. A1. The measured particle number size distributions during eight consecutive type A NPF events at the urban site from the 10 to the 17 August 2010. Among them there were two particle shrinkage events on the 12 and the 16 August 2010.

ACPD
12, 18605–18650, 2012

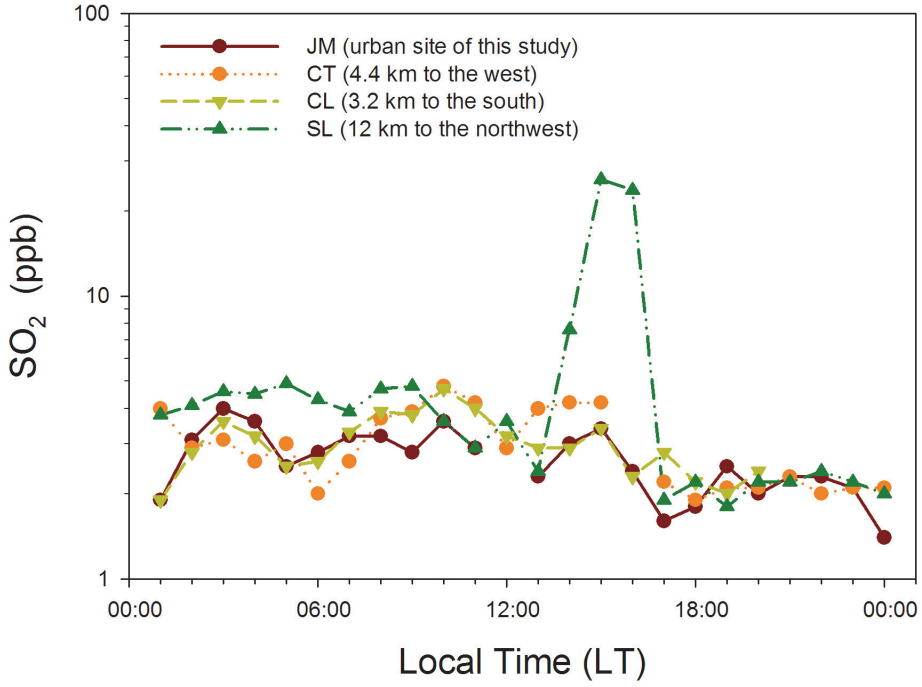

Fig. A2. Diurnal variations of SO_2 measured at the urban site (JM) and three nearby air quality monitoring sites (CT, CL and SL) on the 12 August 2010.

ACPD
12, 18605–18650, 2012